Neuron density is a fundamental determinant of structural connectivity in the primate cerebral cortex

Sarah F. Beul[1], Claus C. Hilgetag[1,2]

[1] Institute of Computational Neuroscience, University Medical Center Hamburg-Eppendorf, 20246 Hamburg, Germany

[2] Neural Systems Laboratory, Department of Health Sciences, Boston University, 02215 Boston, MA, USA

Abstract

Studies of structural brain connectivity have revealed many intriguing features of complex cortical networks. To advance integrative theories of cortical organisation, an understanding of how connectivity interrelates with other aspects of brain architecture is required. Recent studies have suggested that interareal connectivity may be related to macroscopic as well as microscopic features of cortical areas. However, it is unclear how these features are inter-dependent and which most strongly and closely relate to structural corticocortical connectivity. Here, we systematically investigated the relation of many microscopic and macroscopic architectonic features of cortical organization to cortical connectivity, using a comprehensive, up-to-date structural connectome of the primate brain. Importantly, relationships were investigated by multi-variate analyses to account for the interrelations of features. Of all considered factors, the classical architectonic parameter of neuron density was most strongly and consistently related to cortical connectivity, and in conjoint analyses largely abolished effects of other features. These results reveal neuron density as a central architectonic factor of the primate cerebral cortex that is closely related to essential aspects of brain connectivity and which determines further features of the architectonic organization of cortical areas. Our findings integrate several aspects of cortical organization, with implications for cortical development and function.

Introduction

Corticocortical connections underlie information processing in the cerebral cortex. Recent studies of structural brain connectivity have revealed many intriguing features of complex cortical networks. However, the principles by which connections among cortical areas are organized are still poorly understood. Cortical structure has been shown to relate to several fundamental aspects of connectivity, such as the presence or absence of connections or laminar patterns of projection origins and terminations, in different cortical territories as well as different species (Barbas, 1986; Barbas and Rempel-Clower, 1997; Barbas et al., 2005; Medalla and Barbas, 2006; Hilgetag and Grant, 2010; Barbas, 2015; Beul et al., 2015; Goulas et al., 2016; Hilgetag et al., 2016; Beul et al., 2017). Thus, cortical architecture appears to be a determining factor of the organization of cortical connections. These findings have been integrated into a 'structural model' (Barbas, 1986; Barbas, 2015), which explains connectivity based on the relative architectonic differentiation of potentially connected areas. Originally developed qualitatively in the classic studies of Sanides and Pandya (1973), Barbas and coworkers systematically extended the structural model in quantitative studies across a number of cortical systems and connection targets in several mammalian species, including prefrontal, parietal, temporal and occiptal projections, contralateral as well as subcortical projections (e.g., Barbas, 1986; Barbas and Rempel-Clower, 1997; Rempel-Clower and Barbas, 2000; Dombrowski et al., 2001; Barbas et al., 2005; Medalla and Barbas, 2006; Ghashghaei et al. ,2007; Medalla et al., 2007; Hilgetag and Grant, 2010; Goulas et al., 2014; Beul et al., 2015; Goulas et al., 2016; Hilgetag et al., 2016). However, cortical architecture itself is intricate and varies considerably throughout the cortex, as already detailed in classic studies of brain anatomy (Brodman, 1909; von Economo, 1927; 2009). Diverse aspects of cortical structure have been measured at different spatial scales. Such measures comprise macroscopic features, such as the laminar appearance of cortical areas including the thickness of cortical layers and the density and distribution of different types of neurons or glia across layers (Dombrowski et al., 2001; Barbas, 2015), as well as the density of receptors of different neurotransmitter systems (Zilles and Amunts, 2009) or myeloarchitectural features (Nieuwenhuys et al., 2015; Nieuwenhuys and Broere, 2017). In addition, cells within cortical areas have been characterized by a large number of microscopic morphological and physiological measures, such as the density of synpatic spines (Elston et al., 2005; Ballesteros-Yáñez et al., 2006) or firing patterns (Cauli et al., 1997; Dégenètais et al., 2002; Otsuka and Kawaguchi, 2008; Oswald et al., 2013). Given the abundance of possible features, it remains unclear whether there are aspects of cortical structure that carry a higher weight in determining corticocortical connectivity than others. Therefore, we systematically and conjointly analysed multiple architectonic features, to assess their inter-dependence and to

identify which of them were most strongly and closely related to structural cortical connectivity. We contrasted two groups of measures, macroscopic (area-based) structural features as well as microscopic (cellular) morphological measures. Both groups of measures have been linked to the macaque connectome in previous reports (e.g., Scholtens et al., 2014; Hilgetag et al., 2016; Beul et al., 2017), but have not yet been combined in a comprehensive analysis that can disclose their comparative relevance.

The macroscopic measures considered here are neuron density and cortical thickness, as well as the spatial proximity of cortical areas. It has been shown that neuron density consistently relates to essential aspects of corticocortical connectivity, such as the distribution of projection origins and terminations across cortical layers (i.e., laminar projection patterns), the existence of projections, or topological properties of cortical connectivity (Barbas, 1986; Barbas and Rempel-Clower, 1997; Barbas et al., 2005; Barbas, 2015; Hilgetag et al., 2016; Beul et al., 2017). Neuron density is an objective, quantifiable measure of overall cytoarchitectonic differentiation that is characteristic of different cortices (e.g., Dombrowski et al., 2001). Cortical thickness is appealing as a further macroscopic measure because it is relatively easy to measure, also non-invasively. Its relevance to connectivity in healthy and diseased brains has been explored widely (e.g., Lerch et al., 2006; He et al., 2007; Chen et al., 2008; Chen et al., 2011; Tewarie et al., 2014b ; for a review see Evans, 2013; but see Gong et al., 2012), and it is known to be inversely related to neuron density (Von Economo 1927). . In a direct comparison with neuron density, we previously reported cortical thickness to be less informative regarding structural connectivity (Beul et al., 2017). Third, spatial proximity is included, not as a measure of cortical architecture, but as an additional macroscopic feature of physically embedded cortical areas that has been shown to be related to connection existence (Young, 1992; Markov et al., 2013a; Beul et al., 2015; 2017) and strength (Douglas and Martin, 2007; Ercsey-Ravasz et al., 2013), but not laminar projection patterns (e.g., Barbas et al., 2005; Hilgetag et al., 2016).

The cellular morphological measures we consider were obtained for pyramidal cells in cortical layer III (L3), based on extensive immunohistochemical analyses (e.g., Elston and Rosa, 1997). The measures comprise the size of the soma, the total spine count of an average pyramidal neuron, the peak dendritic spine density, and the size of the dendritic tree. These measures have been used to quantify 'pyramidal complexity' in a previous report that found a relation to topological measures of the macaque connectome (Scholtens et al., 2014). In primates, neurons show a tendency to become larger, have more complex dendritic arbors and be more spiny towards the frontal cortex (reviewed in Charvet and Finlay, 2014). Characteristics of cellular morphology are crucial cornerstones for how an area can process incoming information. Spine morphology and spatial arrangement of dendrites directly affect the electrical

and biochemical properties of synapses on pyramidal neurons (reviewed in Spruston, 2008; Yuste, 2010), and spine number and density affect the opportunity for neuronal interactions (reviewed in DeFelipe, 2011). These cellular properties, therefore, directly relate to information processing capabilities of cortical populations, especially with regard to the integration of information from numerous sources (Charvet and Finlay, 2014). In line with areas' position in the interareal circuitry, morphology in prefrontal association areas allows for a broader integration of inputs (Bianchi et al., 2013; Buckner and Krienen, 2013). Moreover, variation in cellular morphological characteristics across species presumably also reflects differences in the complexity of cortical circuits and specifics of information processing, which plausibly have wide-ranging implications for cognition, memory and learning (DeFelipe, 2011). Below, we contrast the relative contribution of each of these seven measures for characterizing inter-areal connections in the macaque cerebral cortex. We show that not all measures are equally relevant, and that neuron density in particular emerged as the most essential and informative feature for explaining the organization of the connectome.

Materials and Methods

We first introduce the connectome data set for the macaque cortex and then present the investigated structural measures. Subsequently, we describe statistics and procedures used in the analyses.

Connectivity data

We analysed an extensive, up-to-date set of anatomical tracing data in the macaque cortex (Markov et al., 2014). Based on injections of retrograde tracer in 29 areas, the dataset provided information on 2610 corticocortical connections between 91 areas (represented in the M132 atlas, Markov et al., 2014). For projections found to be present, projection strength was given as the fraction of labeled neurons outside of the injected region (FLNe), thus normalizing the number of projection neurons between two areas to the total number of labeled neurons for the respective injection, as done previously (e.g., Barbas and Rempel-Clower, 1997; Medalla and Barbas, 2006). To assess the relation of the structural measures with projection existence, we transformed projection strength to a binary measure (absent / present). To assess the relation of the structural measures with projection strength, we considered the natural logarithm, ln(FLNe). The use of a logarithmic scale was indicated, since the most extreme FLNe value was more than three standard deviations above the mean of the considered neuron densities (Buzsáki and Mizuseki, 2014). In addition, we analyzed the laminar patterns of projection origins for this data set (Chaudhuri

et al., 2015). The fraction of labeled neurons originating in supragranular layers (N_{SG}%) was provided for 1602 present projections from all injected areas. Specifically, N_{SG}% was computed as the number of supragranular labeled neurons divided by the sum of supragranular and infragranular labeled neurons. To relate N_{SG}% to the undirected measure of Euclidean distance, we also transformed it to an undirected measure of inequality in laminar patterns, $|N_{SG}\%|$, where $|N_{SG}\%| = |N_{SG}\% - 50| * 2$. Values of N_{SG}% around 0% and 100% thus translated to larger values of $|N_{SG}\%|$, indicating a more pronounced inequality in the distribution of origins of projection neurons between infra- and supragranular layers and hence deviation from a columnar (bilaminar) pattern of projection origins. We based our analyses regarding N_{SG}% on the subset of 1132 projections comprising more than 20 neurons (neuron numbers for each projection are provided in Markov et al., 2014). Thus, we excluded very weak projections for which assessment of the distribution of projection neurons in cortical layers was not considered reliable (cf. Barbas et al., 2005).

The data set contains the 29x29 subgraph of injected areas for which all possible connections have been examined. To assess area degree, we considered only areas within this edge-complete subgraph, computing the degree of each area as the sum of the number of its afferent and efferent projections, as reported previously (Beul et al., 2017).

Structural measures

Next, we introduce the investigated seven area-based and cellular morphological measures, grouped by their spatial (macroscopic or microscopic) scale (Figure 1).

Macroscopic measures

Neuron density. We used an unbiased quantitative stereologic approach to estimate neuron density from immunohistochemically stained sections of macaque cortex using a microscope-computer interface (StereoInvestigator, MicroBrightField Inc., Williston, VT). The neuron density measurements used here have been partly published before (Dombrowski et al., 2001; Hilgetag et al., 2016; Beul et al., 2017). In total, neuron density measures were available for 48 of the 91 areas in the M132 parcellation. We quantified how similar areas were in their neuron density by computing the log-ratio of neuron density values for each pair of areas (which is equivalent to the difference of the logarithms of the area densities). Specifically, log-ratio$_{density}$ = ln(density$_{source\ area}$ / density$_{target\ area}$). This procedure enabled us to directly relate each sampled projection to the density ratio of its source- and target-area. The use of a logarithmic scale was indicated, since the

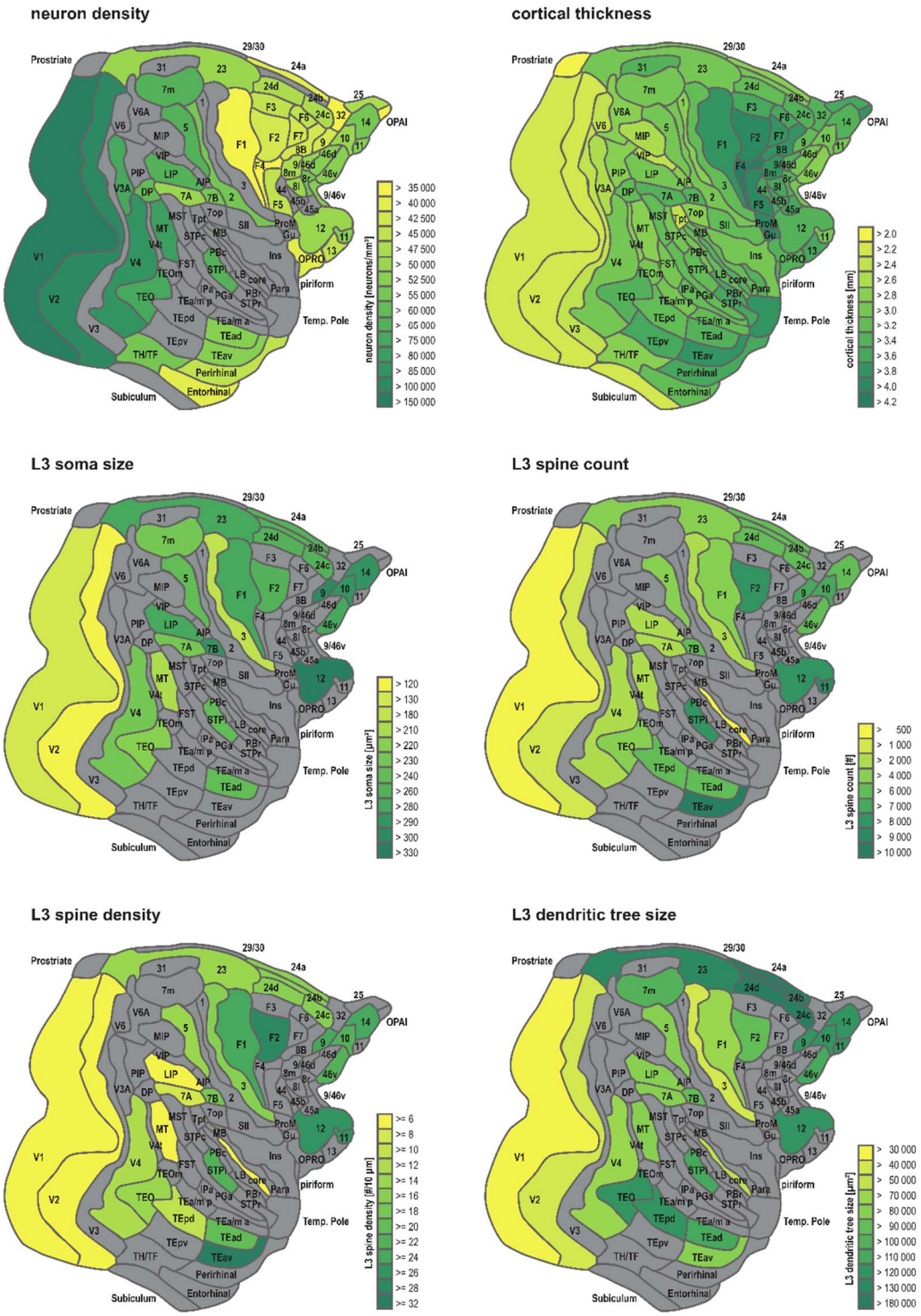

Figure 1. Variation of cytoarchitectonic features across the primate cortex.

Variation of neuron density, overall cortical thickness, L3 neuron soma size, L3 dendritic spine count, L3 dendritic spine density and L3 dendritic tree size depicted on the M132 parcellation (Markov et al., 2014). For grey areas, no values were available. See Table 1 for correspondences between areas in the M132 parcellation and alternative parcellations. Abbreviations as in Markov et al. (2014).

most extreme value of the neuron density measures was more than three standard deviations above the mean of the considered neuron densities (Buzsáki and Mizuseki, 2014). For analyses which required considering an undirected equivalent of the actual neuron density ratio, we used the absolute value of the log-ratio, $|\text{log-ratio}_{\text{density}}|$. More detailed descriptions of the acquisition of the neuron density measurements have been published elsewhere (Hilgetag et al., 2016; Beul et al., 2017).

Cortical thickness. Cortical thickness data were extracted from an anatomical T1-weighted magnetic resonance (MR) brain scan of one male adult macaque monkey (*Macaca mulatta*). MR data were acquired on a 3 Tesla Philips Achieva MRI scanner using a three-dimensional magnetization prepared rapid acquisition gradient-echo (3DMPRAGE) sequence with 0.6 mm isotropic voxels (130 slices, TR = 7.09 ms, TE = 3.16 ms, FOV = 155 x 155 mm^2). Cortical reconstruction and volumetric segmentation was performed using the Freesurfer image analysis suite (http://surfer.nmr.mgh.harvard.edu/). The resulting surface reconstruction was registered to the M132 atlas (Markov et al., 2014) using the Caret software (http://www.nitrc.org/projects/caret/; van Essen et al., 2001). Cortical thickness was then extracted for all 91 areas in both hemispheres using Freesurfer. Here, we report results for mean thickness values of the left and right hemisphere. We quantified how similar areas were in their thickness across the cortex by computing the log-ratio of thickness values for each pair of areas, analogous to the log-ratio of neuron density, where $\text{log-ratio}_{\text{thickness}} = \ln(\text{thickness}_{\text{source area}} / \text{thickness}_{\text{target area}})$. We transformed the log-ratio of cortical thickness to an undirected equivalent, $|\text{log-ratio}_{\text{thickness}}|$, where appropriate. These measures were also used in previous analyses (Beul et al., 2017).

Spatial proximity. To quantify the spatial proximity of cortical areas, we used the Euclidean distance between the mass centers of all 91 areas, obtained from the Scalable Brain Atlas (http://scalablebrainatlas.incf.org). This widely used interval measure of projection length represents a pragmatic estimate of projection length (e.g., Salvador et al., 2005; Achard et al., 2006; Bassett et al., 2008; Vertés et al., 2012; Alexander-Bloch et al., 2013; Goñi et al., 2014; Tewarie et al., 2014a).

Cellular morphological measures

Measures of cellular morphology were reported by Elston and colleagues (Elston and Rosa, 1997; Elston and Rosa, 1998; Elston et al., 1999a; Elston et al., 1999b; Elston, 2000; Elston et al., 2001; Elston and Rockland, 2002; Elston et al., 2005; Elston et al., 2010; Elston et al., 2011a; Elston et al., 2011b). Specifically, Elston and colleagues measured four aspects of L3 pyramidal neuron morphology across the macaque cortex: the size of the cell soma (soma size),

the average total spine count on the basal dendritic tree (spine count), the peak density of dendritic spines (spine density), and the size of the basal dendritic tree (dendritic tree size).

Table 1 gives an overview of the correspondence between the parcellation used by Elston and colleagues and the M132 parcellation, as well as the relevant reports. Specifically, in the M132 parcellation, soma size was available for 25 areas, spine count and spine density for 28 areas, and dendritic tree size for 29 areas.

To quantify how similar areas were in these four morphological measures across the cortex, we computed the difference of their values for each pair of areas, where $\Delta_{\text{morphological measure}} = \text{measure}_{\text{source area}} - \text{measure}_{\text{target area}}$). This resulted in $\Delta_{\text{soma size}}$, $\Delta_{\text{spine count}}$, $\Delta_{\text{spine density}}$, and $\Delta_{\text{tree size}}$. Each of these difference measures was converted to an undirected variable by computing its absolute value, $|\Delta_{\text{soma size}}|$, $|\Delta_{\text{spine count}}|$, $|\Delta_{\text{spine density}}|$, and $|\Delta_{\text{tree size}}|$, where appropriate.

Statistical tests

To test groups of projections for equality in their associated structural measures, we computed two-tailed independent samples t-tests and report the t-statistic t, degrees of freedom df and the associated measure of effect size r, where $r = (t^2 / (t^2+df))^{1/2}$. To assess relations between structural measures, we computed Pearson's correlation coefficient r. All tests were conducted with a pre-assigned two-tailed significance level of $\alpha = 0.05$. These analyses were performed using Matlab R2012b (The MathWorks, Inc., Natick, MA, United States).

We performed binary logistic regression analyses using projection existence as the binary dependent variable and different combinations of the relative structural measures as covariates. Specifically, we considered $|\text{log-ratio}_{\text{density}}|$, $|\text{log-ratio}_{\text{thickness}}|$, Euclidean distance, $|\Delta_{\text{soma size}}|$, $|\Delta_{\text{spine count}}|$, $|\Delta_{\text{spine density}}|$, and $|\Delta_{\text{tree size}}|$. The relative structural measures were converted to z-scores, so that the resulting regression coefficients were standardized. We also included a constant in each model. All covariates were entered into the model simultaneously. We report the standardized regression coefficients, the Wald statistic *W*, and its associated p-value. These analyses were performed using SPSS Statistics 21 (IBM Corporation, Armonk, NY, United States).

Results

Macroscopic and microscopic morphological measures are interrelated

The macroscopic and microscopic morphological measures were strongly correlated with each other, with the possible exception of dendritic tree size. When the standard significance threshold of $\alpha = 0.05$ was applied, all

correlations but one (dendritic spine density with dendritic tree size) were statistically significant. Using a Bonferroni correction for multiple tests resulted in an adjusted significance threshold of $\alpha_{adj} = 0.05/10 = 0.005$. Under this criterion, the significance of all but one correlation remained unaffected: Only the correlation of dendritic tree size with soma size lost statistical significance. Table 2 summarizes these results. Furthermore, Figure 2 gives a visual overview of the observed relations between these five measures.

Neuron density is most consistently related to the existence of projections

To assess whether the seven structural measures were distributed differently across absent and present projections, we computed independent samples t-tests. These showed that connected cortical areas had smaller neuron density ratios and cortical thickness ratios than areas that were not linked. Similarly, linked areas were separated by smaller

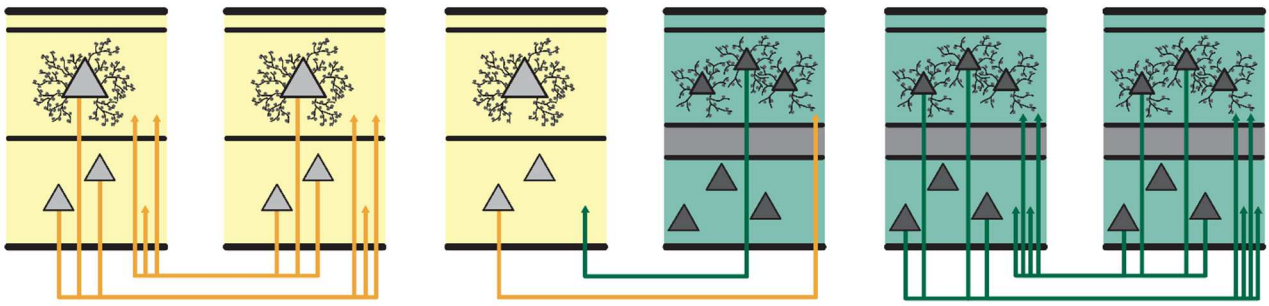

Figure 2. Projection patterns in context of structural variation.

Less architectonically differentiated cortical areas (agranular, yellow) are characterized by lower neuron density and different morphology of layer 3 pyramidal cells than more strongly differentiated areas (eulaminate, green). Specifically, as shown in Table 2, higher neuron density correlates with smaller size of the soma and the dendritic tree as well as with lower total spine count and peak spine density. Laminar patterns of projection origin are indicated as observed in this report (cf. Table 6) and consistent with the structural model of cortical connectivity (Barbas, 1986; Barbas, 2015). Connections between areas of similar architectonic differentiation show a bilaminar projection origin pattern (agranular to agranular, left panel, and eulaminate to eulaminate, right panel), while connections between areas of distinct differentiation show a skewed unilaminar projection pattern, with projections originating predominantly in the infragranular or supragranular layers (agranular to eulaminate and eulaminate to agranular, middle panel).

distances than unconnected areas. The differences between areas in the four morphological measures were also smaller if areas were connected than if no connection had been found. Of all the tested structural features, effect size was largest for neuron density ratio. These results are summarized in Figure 3 and Table 3.

We used binary logistic regression to probe how well the structural measures could account for the existence of projections (Figure 4). First, we combined the structural measures as they were used previously: We included either (1) all macroscopic measures (absolute neuron density ratio, absolute cortical thickness ratio, and Euclidean distance) or (2) all cellular morphological measures (absolute soma size difference, absolute spine count difference, absolute spine density difference, and absolute dendritic tree size difference) as covariates. Second, we included (3) all seven measures in conjunction as covariates. As presented in Table 4, when only macroscopic measures were considered (1), both neuron density ratio and Euclidean distance contributed significantly to the model performance. If the cellular morphological measures were considered on their own (2), only soma size difference

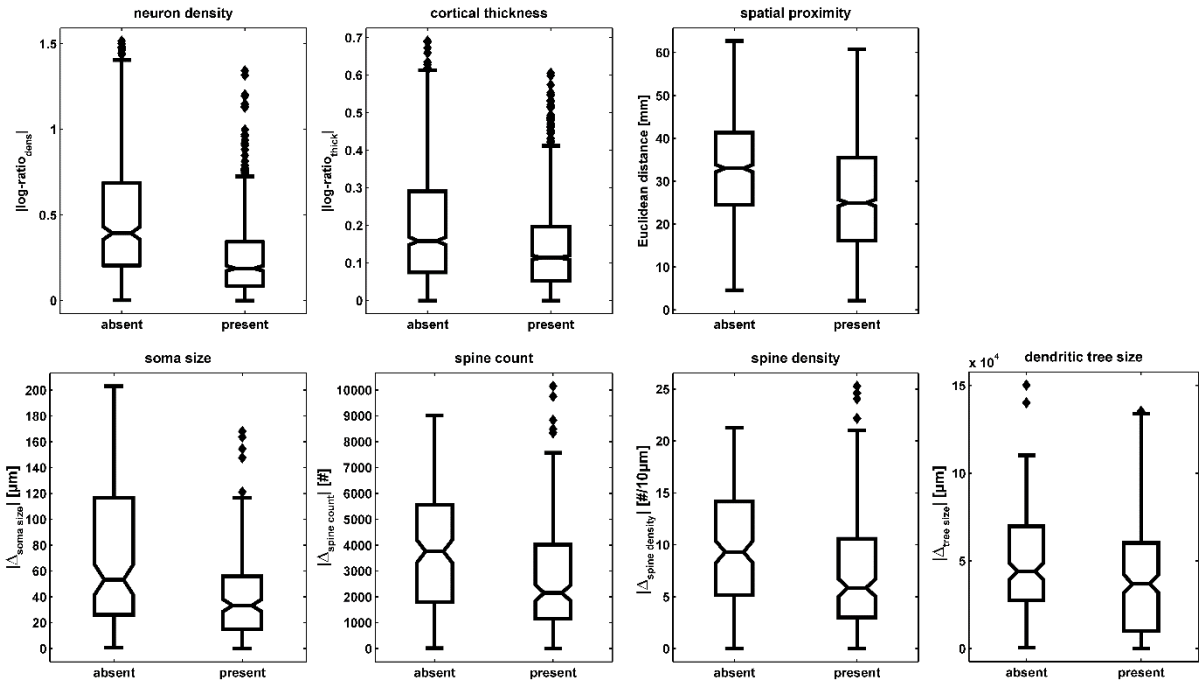

Figure 3. Relative structural measures differ between connected and unconnected pairs of areas.

Box plots show distributions of absolute values of relative structural measures for area pairs without (absent) and with (present) a linking projection. Indicated are median (line), interquartile range (box), data range (whiskers) and outliers (diamonds, outside of 2.7 standard deviations). See Table 3 for a summary.

contributed significantly. If, however, all seven measures were included as covariates (3), neuron density ratio and Euclidean distance continued to contribute significantly, while soma size difference did not. This result suggests that the neuron density ratio is more fundamental than soma size in explaining the existence of connections. To test this hypothesis explicitly, we combined a reduced number of covariates and found that soma size did not contribute significantly when combined just with the neuron density ratio (4), but did when combined only with Euclidean distance (5). These observations further support our conclusion that neuron density was the structural measure that principally related to the existence of connections.

Neuron density and distance are consistently related to projection strength

The strength of cortical projections has been shown to diminish with greater distance of the connected areas (e.g., Ercsey-Ravasz et al., 2013). Here, we related all area-based as well as cell-based measures to the strength of projections, ln(FLNe). Figure 5 and Table 5 show that each measure individually was weakly to moderately correlated with projection strength, with the exception of dendritic tree size difference. Since most measures were correlated with each other, we entered all measures into a partial Pearson correlation to assess their relative contribution to projection strength if the other measures were controlled for. As shown in Table 5, even when all other measures were controlled for, neuron density ratio and Euclidean distance retained their correlation to projection strength with only a slight change in the correlation coefficient r. The third measure that remained significantly correlated with projection strength was spine density difference. The correlations for the remaining four measures were not significant if all measures were considered simultaneously.

Neuron density is consistently related to laminar patterns of projection origins

Our analyses of the extensive projection origin data provided in Chaudhuri et al. (2015) show that neuron density is consistently related to this feature of corticocortical projections. As seen from Figure 6 and Table 6, all directed measures were moderately to strongly correlated with the laminar pattern of projections expressed as N_{SG}%. However, in a partial Pearson correlation of N_{SG}% with all measures, except Euclidean distance, only neuron density ratio and spine count difference retained significance. Although the correlation with spine density difference was below the significance threshold, the correlation coefficient changed its sign while remaining at a moderate

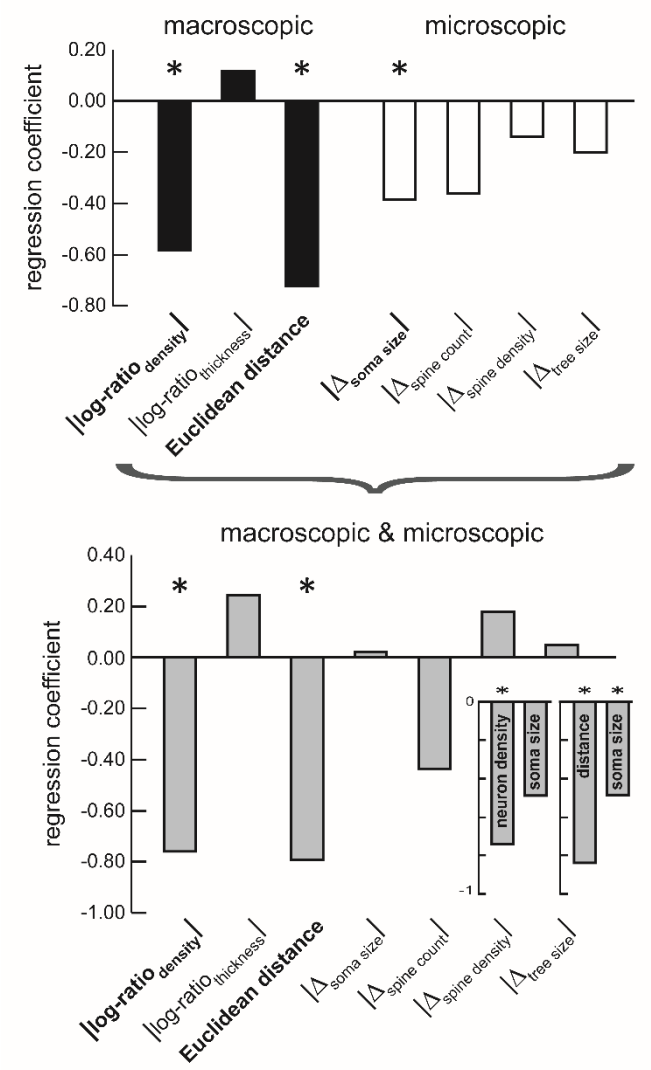

Figure 4. Classification of connection existence by logistic regression.

Regression coefficients for logistic regressions including either all macroscopic measures (top left, black bars) or cellular morphological measures (top right, white bars). Only a subset of structural measures significantly contributed to classification performance (indicated by stars, $p < 0.05$). Across all regression analyses, absolute neuron density ratio and Euclidean distance consistently emerged as meaningful predictors (bottom, grey bars). Absolute soma size difference, which contributed significantly within the subset of morphological measures, was no relevant predictor if absolute neuron density ratio was included as well, but did remain so in combination with Euclidean distance (see inset). See Table 4 for regression coefficients and test statistics of all regression analyses.

magnitude, indicating that the correlation was volatile and not reliable. Euclidean distance, an undirected measure, was tested for a correlation with an indicator of deviation from bilaminar projection patterns, $|N_{SG}\%|$, and did not reach significance. To test the effect of additionally controlling the partial Pearson correlation for Euclidean distance, we computed a partial Pearson correlation of $|N_{SG}\%|$ with Euclidean distance as well as the absolute values of the other six measures. Here, absolute neuron density ratio again remained significant at a moderate magnitude. The other two measures that were significant in this correlation were absolute soma size difference and absolute spine count difference. Here, the change of sign of the correlation coefficients was due to the applied transformations of the data compared to the individual correlations and not indicative of a volatile correlation. In conclusion, the variables found to be significantly associated with the laminar pattern of projections across all variations of correlating the measures were neuron density ratio and spine count difference.

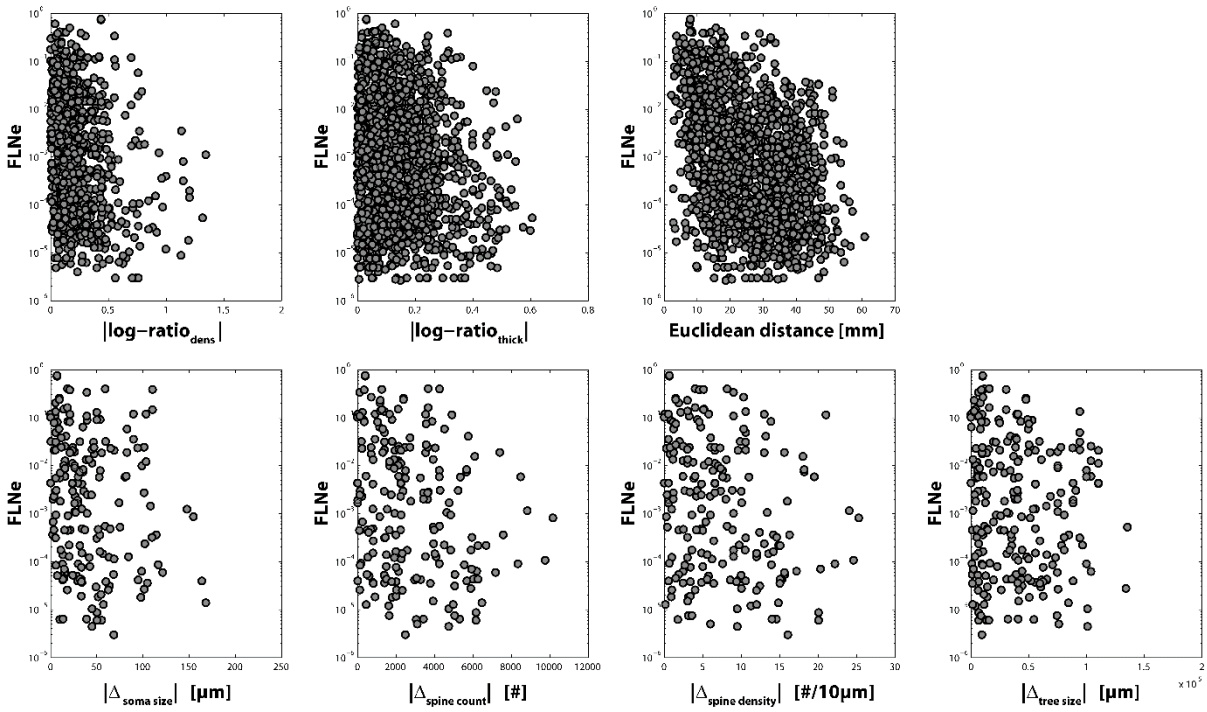

Figure 5. Projection strength varies with relative structural measures.

Projection strength for individual projections, FLNe, is shown across absolute values of relative structural measures. See Table 5 for correlation statistics.

Neuron density is correlated with the number of connections of cortical areas

As in previous reports (Scholtens et al., 2014; Beul et al., 2017), we examined the correlation of structural measures with area degree, the number of connections a cortical region maintains. We tested six of the seven measures. Spatial proximity was excluded, because Euclidean distance is inherently relational and cannot be related to a measure pertaining to a single area. Figure 7 and Table 7 show that of the six tested measures, only neuron density and cortical thickness were significantly correlated with area degree (these two correlations were reported previously in Beul et al., 2017). Using a Bonferroni correction for multiple tests results in an adjusted significance threshold of $\alpha_{adj} = 0.05/6 = 0.0083$. Under this criterion, the correlation of cortical thickness lost significance, leaving neuron density as the only structural measure that was significantly correlated with area degree. In a partial Pearson correlation, none of the six measures retained a significant correlation with area degree. However, controlling for all measures in the partial correlation reduced the number of available data points to 13 for all measures (cf. Figure 7, black data points). The increase in the p-value for the correlation between neuron density and degree to 0.08 and the ensuing loss of significance might have been caused by the decrease in the number of data points for neuron density (from 24 to 13), rather than an actual explanation of the effect through the other measures. By comparison, only one or two data points were lost for each of the four morphological measures. For two of them, soma size and spine density, the exclusion of one data point was sufficient to invert the sign of their correlation with area degree (at a moderate to strong magnitude of the correlation coefficient), which further suggests that their relation to area degree is not systematic.

Discussion

The extent to which cortical architecture determines the organization of structural connectivity in the cerebral cortex has been examined from a variety of perspectives (Hilgetag and Grant, 2010; Scholtens et al., 2014; Beul et al., 2015; Hilgetag et al., 2016; Beul et al., 2017; for a review see Barbas, 2015). Here, we explored the relative explanatory power of seven structural measures with regard to the organization of corticocortical connections in the macaque cortex. These architectonic measures were examined individually in previous reports (Scholtens et al., 2014; Hilgetag et al., 2016; Beul et al., 2017) and fall into two broad categories: The first group consists of the macroscopic measures of neuron density, cortical thickness, as well as spatial proximity. The second group comprises the microscopic cellular morphological measures of soma size, total dendritic spine count, peak dendritic spine density, and dendritic tree size, all measured in L3 cortical pyramidal neurons. We considered these measures

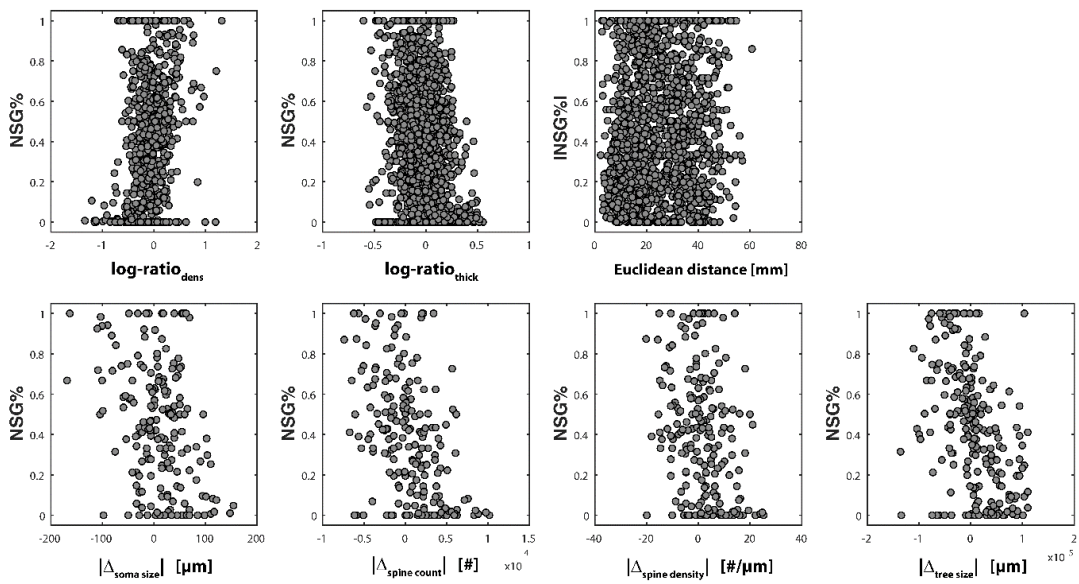

Figure 6. Laminar projection patterns vary with relative structural measures.

Fraction of supragranularly labelled neurons for individual projections, N_{SG}%, is shown across relative structural measures. Note that for Euclidean distance, the measure of deviation from columnar laminar patterns |N_{SG}%| is shown instead. See Table 6 for correlation statistics.

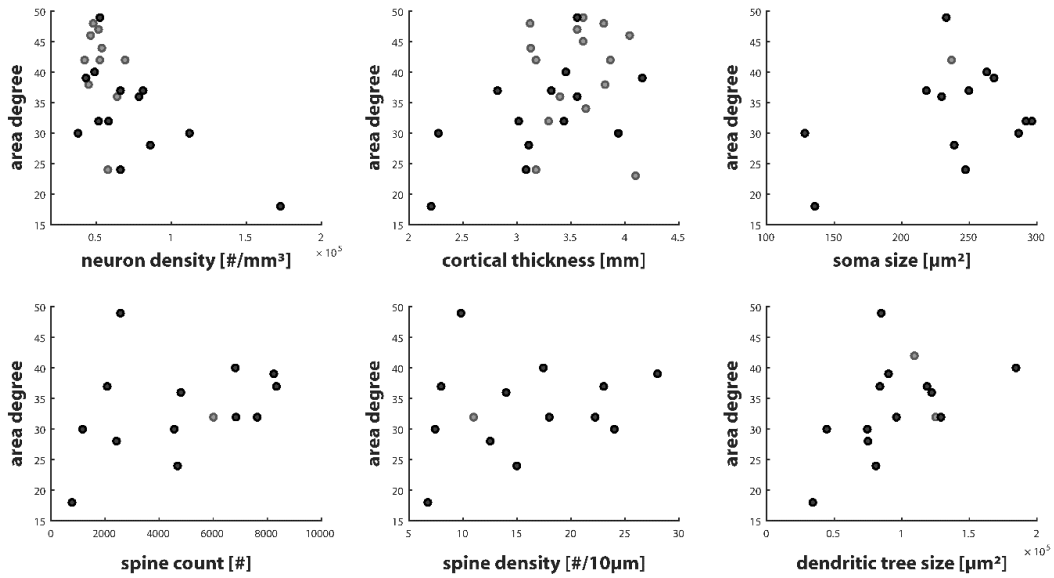

Figure 7. Area degree varies with structural measures.

The number of projections an area maintains, area degree, is shown across structural measures for each area. See Table 7 for correlation statistics. All data points (black and grey) were considered in the individual correlations reported there, while only black data points were considered in the partial correlation.

in conjunction, to assess how they relate to each other as well as to establish which of them carried the most weight for explaining fundamental organizational aspects of the primate cortical connectome.

We found that all morphological measures are strongly correlated with each other as well as with neuron density (Table 2). Moreover, all seven measures diverged depending on whether areas were linked by a projection or not (Figure 3, Table 3). This finding raises the question of whether all of these measures equally contribute to the discrimination of corticocortical connectivity, or whether some of them are redundant, being dependent on other factors, and supply no additional information. Systematic analysis by multivariate logistic regression revealed that, of the cellular morphological measures, relative L3 pyramidal cell soma size carried the largest amount of information (Table 4, (2)). However, its contribution diminished below the significance threshold, if the macroscopic, area-based measures were also included as covariates (Table 4, (3)). The effect was specifically due to the inclusion of neuron density as a covariate, since it did not occur if the only other covariate was Euclidean distance (Table 4, (4) and (5)). This finding suggests that neuron density was the most informative measure regarding the existence of projections.

We further found that neuron density ratio and Euclidean distance were correlated with projection strength, even if all other structural measures were controlled for (Table 5). Of the four cellular measures, only spine density difference was significantly correlated with projection strength in this case. Additionally, the laminar patterns of projection origins were correlated with the neuron density ratio and spine count difference (Table 6), but not consistently with the other five structural measures. Moreover, neuron density was the only structural measure that was significantly correlated with the topological measure of area degree, that is, the number of connections of cortical areas (Table 7).

In summary, our analyses indicate that, while the cellular morphological measures and the area-based measure neuron density are closely related, neuron density is a more essential predictor of basic features of corticocortical connectivity (projection existence and strength, laminar projection patterns and area degree) than the cellular morphological measures. This finding is consistent with previous reports which demonstrated that neuron density provided a more characteristic ‘fingerprint’ of the cytoarchitecture of cortical areas than other architectonic measures (Dombrowski et al., 2001), as well as with reports showing that a close relation between architectonic differentiation and corticocortical connectivity could also be observed in different mammalian species such as the cat and mouse (Hilgetag and Grant, 2010; Beul et al., 2015; Goulas et al., 2016).

Developmental mechanisms may regulate the covariation of architectonic measures

Systematic, joint variation of different features of cellular morphology has been observed between cortical regions of particular mammalian species, as well as across species. In primates, a higher number and higher density of spines and more complex dendritic arbors have been reported in prefrontal cortices compared to motor or sensory cortices (Elston, 2003; Elston, 2007; Elston et al., 2011a; Bianchi et al, 2013). In mouse cortex, spine density in the prelimbic and infralimbic fields is twice as high as in the remaining cortex (Ballesteros-Yáñez et al., 2010), and spine size varies across the cortex (Benavides-Piccione et al., 2002). Here, we have shown that these gradual changes in cell morphology are aligned with the overall degree of architectonic differentiation observed in cortical areas. Moreover, it has been noted that variation in both cellular architecture and neuron numbers is well aligned with developmental gradients (Charvet and Finlay, 2014; Charvet et al., 2015). This link has been corroborated by findings in the human cortex which directly traced the systematic architectonic variation of the cortex to the timing of development (Barbas and García-Cabezas, 2016). Across species, human spines were shown to be larger as well as longer and to be present at higher densities than synaptic spines in mouse cortex (Benavides-Piccione et al., 2002). More generally, dendritic complexity has been shown to successively increase from new world monkeys to old world monkeys to hominids, being exceptionally pronounced in the human cortex (Elston et al., 2003; Elston, 2007; Bianchi et al., 2013; reviewed in Charvet and Finlay, 2014). This observation is in correspondence with an increase in overall neuron density as developmental time schedules lengthen and brain size increases (reviewed in Caviness et al., 2008; Charvet and Finlay, 2014). In summary, multiple dimensions of cellular morphology appear to be tightly coupled, matching the overall degree of area differentiation as well as variation in developmental timing. Together, these observations point towards a precise orchestration of cell specification during ontogenesis, such that morphological, microscopic features of neurons are attuned to the macroscopic architectonic differentiation of an area as a whole.

Additionally, physical self-organization may play a role in shaping the covariation of overall architectonic differentiation, determined by spatiotemporal developmental gradients, and morphological measures. Assuming that neurons and neuropil are packed into the available cortical volume as tightly as possible, approximating maximum volume packing (e.g., Chklovskii et al., 2002), the cellular morphological features would be expected to adjust to neuron density quite as is observed. In particular, a higher density of neurons would lead to smaller somata, less extensive dendritic arborization, and possibly also dendrites that are less spiny.

Functional implications

It appears that local cortical architecture, connection features of a cortical area, as well an area's functional role within the cortical network are tightly interrelated. First, laminar projection patterns place origins and terminations in laminar microenvironments appropriate for the type of information exchange between pairs of cortical areas. As noted before, the observed anatomical distinctions between laminar patterns of projections connecting areas of varying relative differentiation likely reflect differences in information processing (e.g., Barone et al, 1995). Specifically, projections that propagate information towards more abstract and multi-modal processing regions show a different laminar composition than projections that feed back the results of information integration to areas closer to the sensory periphery, affecting behaviour by modulating information processing (reviewed in Batardière et al., 1998; Buckner and Krienen, 2013; Harris and Shepherd, 2015). These anatomical distinctions are accompanied by differences in electrophysiological signatures associated with the respective pathways (Bastos et al., 2015). Moreover, neurons in infragranular and supragranular layers have been shown to possess different physiological (Lagae et al., 1989; Nowak et al., 1995; Raiguel et al., 1995) as well as histochemical characteristics (Hof et al., 1996; 1997). These observations are functionally relevant, since even small variations in cell-intrinsic properties can effect substantial differences in the computations performed by otherwise similar circuits (Harris and Shepherd, 2015). The modulation of information processing is accomplished through precisely targeted inputs (reviewed in Larkum, 2013), so that exerting a modulatory effect does not require an accumulation of incoming connections, but can be achieved by relative weak inputs. This situation is in contrast to driving inputs delivered by feedforward projections that originate predominantly in supragranular layers. In a comparison of feedforward and feedback projections that were similar in their absolute deviation from bilaminar projection patterns (i.e., $|N_{SG}\%|$), feedforward projections were reported to be stronger than feedback projections (Markov et al., 2013b), illustrating diverging requirements for driving and modulating influences. Similarly, feedforward projections terminating in middle cortical layers were shown to have larger boutons, and hence potentially stronger drive, than projections terminating outside the middle layers (Germuska et al., 2006). Connection features thus correspond well to the functional roles of connected areas. Second, in a complementary way, the intrinsic processing capabilities of cortical areas are, to a large extent, determined by local characteristics of cellular morphology. Cellular morphological properties and the functional roles of cortical areas, thus, also appear attuned to each other. Finally, the relation between cortical architecture and connection features completes the three interactive aspects. The observations integrated into the structural model extensively describe this interrelation. Moreover, the dependence of cortical connections on relative

architectonic differentiation formalized in the structural model affords deeper insight into multiple aspects of the organization of cortical connectivity (reviewed in Barbas, 2015; Hilgetag et al., 2016). For example, the arrangement of areas by relative differentiation is consistent with onset latencies in the visual system (Petroni et al., 2001) and an ordering of areas inferred from their functional interactions in different frequency bands (Bastos et al., 2015). Laminar projection patterns indicate that areas of weak differentiation (limbic cortices) feed back information to more strongly differentiated areas (Barbas, 1986; Barbas and Rempel-Clower, 1997), placing them in a central position in the cortical network. This observation is consistent with their involvement in the default mode network (Raichle, 2011) as well as a suggested link to functional conscious access (Dehaene et al., 1998; 2011). The structural model also pertains to disruptions of specific pathways in diseases, for example autism (Zikopoulos and Barbas, 2010; 2013). In summary, the strong correlation between the laminar origins of interareal projections and relative architectonic differentiation is closely intertwined with the functional relevance of a given projection. It reflects the seamless integration of the functional interplay of areas with local morphological properties and their associated intrinsic processing capabilities.

Limitations of the explanatory power of architectonic factors

The present results show that a characteristic indicator of the overall degree of architectonic differentiation, neuron density, is well suited for accounting for structural connections within the global, macro-scale cortical connectome of the primate. In contrast, more fine-grained structural aspects of the cortex, such as the cellular morphological features considered here, convey less information on the connectional features of areas, appearing as derivate properties determined mostly by overall regional differentiation. However, it should be noted, that the considered morphological measures were solely acquired for supragranular cortical layer 3 and characterize only pyramidal neurons. Hence, these measures were not designed to comprehensively capture the intrinsic architectonic organization of cortical areas. Considering such inherent differences between the measures, it is plausible that neuron density, as an overall characterization of area structure, correlates better with the areas' macroscopic connectivity properties, as found. If a more detailed characterization of cellular morphology was available, for example through equivalent morphological measures obtained from the infragranular layers, the morphology might be captured by a summary measure (e.g., ratios across different laminar compartments) which could be used to characterize overall cortical architecture. Such a more detailed characterization of cellular morphology might then correlate with macroscopic properties of the connectome as well as neuron density.

Conclusions

Cortical structure has been shown to relate to fundamental aspects of the organization of corticocortical connections (Barbas, 1986; Barbas and Rempel-Clower, 1997; Barbas et al., 2005; Medalla and Barbas, 2006; Hilgetag and Grant, 2010; Barbas, 2015; Beul et al., 2015; Hilgetag et al., 2016; Beul et al., 2017) and appears integral for understanding cortical connectivity. However, not all structural measures are equally informative on connectivity, as we have shown in conjoint analyses of multiple macro- and microscopic properties here, as well as in previous reports (Dombrowski et al., 2001; Hilgetag et al., 2016; Beul et al., 2017). We found that neuron density, a basic (and classic) macroscopic indicator of overall architectonic differentiation of cortical areas more consistently related to multiple features of the macaque connectome than four microscopic morphological measures. These cellular measures, moreover, were themselves closely related to neuron density. Thus, it can be speculated whether these microscopic properties are developmentally attuned to overall architectonic differentiation of the cortex. Such an alignment might result from neurodevelopmental mechanisms combining genetic determination of regionally specific gradients with processes of physical self-organization, such as maximum volume packing, resulting in trade-offs between cell density and cell size as well as cellular complexity. Neuron density, thus, links the macroscale and microscale architectonic and connectional organization of cortical areas and allows integrating the overall structural differentiation of areas with features of cellular morphology as well as with the existence, density and laminar characteristics of corticocortical connections. This insight may be a significant step towards the development of advanced across-scales models of cortical organization and function.

Acknowledgements

We thank Helen Barbas for providing MR data and Konrad Wagstyl for the extraction of cortical thickness values from MR data. SFB and CCH were supported by DFG Collaborative Research Center Grant SFB 936/A1. Address correspondence to Claus C. Hilgetag, Institute of Computational Neuroscience, University Medical Center Eppendorf, Martinistr. 52, 20246 Hamburg, Germany. Email: c.hilgetag@uke.de.

References

Achard S, Salvador R, Whitcher B, Suckling J, Bullmore ET. 2006. A Resilient, Low-Frequency, Small-World Human Brain Functional Network with Highly Connected Association Cortical Hubs. J Neurosci. 26:63–72.

Alexander-Bloch AF, Vértes PE, Stidd R, Lalonde F, Clasen L, Rapoport J, Giedd J, Bullmore ET, Gogtay N. 2013. The Anatomical Distance of Functional Connections Predicts Brain Network Topology in Health and Schizophrenia. Cerebral Cortex. 23:127–138.

Ballesteros-Yáñez I, Benavides-Piccione R, Bourgeois J-P, Changeux J-P, DeFelipe J. 2010. Alterations of cortical pyramidal neurons in mice lacking high-affinity nicotinic receptors. PNAS. 107:11567–11572.

Ballesteros-Yáñez I, Benavides-Piccione R, Elston GN, Yuste R, DeFelipe J. 2006. Density and morphology of dendritic spines in mouse neocortex. Neuroscience. 138:403–409.

Barbas H. 1986. Pattern in the laminar origin of corticocortical connections. J Comp Neurol. 252:415–422.

Barbas H. 2015. General Cortical and Special Prefrontal Connections: Principles from Structure to Function. Annual Review of Neuroscience. 38:269–289.

Barbas H, García-Cabezas MÁ. 2016. How the prefrontal executive got its stripes. Current Opinion in Neurobiology. 40:125–134.

Barbas H, Hilgetag CC, Saha S, Dermon CR, Suski JL. 2005. Parallel organization of contralateral and ipsilateral prefrontal cortical projections in the rhesus monkey. BMC Neuroscience. 6:32.

Barbas H, Rempel-Clower NL. 1997. Cortical structure predicts the pattern of corticocortical connections. Cereb Cortex. 7:635–646.

Barone P, Dehay C, Berland M, Bullier J, Kennedy H. 1995. Developmental remodeling of primate visual cortical pathways. Cereb Cortex. 5:22–38.

Bassett DS, Bullmore ET, Verchinski BA, Mattay VS, Weinberger DR, Meyer-Lindenberg A. 2008. Hierarchical Organization of Human Cortical Networks in Health and Schizophrenia. J Neurosci. 28:9239–9248.

Bastos AM, Vezoli J, Bosman CA, Schoffelen J-M, Oostenveld R, Dowdall JR, De Weerd P, Kennedy H, Fries P. 2015. Visual Areas Exert Feedforward and Feedback Influences through Distinct Frequency Channels. Neuron. 85:390–401.

Batardière A, Barone P, Dehay C, Kennedy H. 1998. Area-specific laminar distribution of cortical feedback neurons projecting to cat area 17: Quantitative analysis in the adult and during ontogeny. J Comp Neurol. 396:493–510.

Benavides-Piccione R, Ballesteros-Yáñez I, DeFelipe J, Yuste R. 2002. Cortical area and species differences in dendritic spine morphology. Journal of Neurocytology. 31:337–346.

Beul SF, Barbas H, Hilgetag CC. 2017. A Predictive Structural Model of the Primate Connectome. Scientific Reports. 7:43176.

Beul SF, Grant S, Hilgetag CC. 2015. A predictive model of the cat cortical connectome based on cytoarchitecture and distance. Brain Struct Funct. 220:3167–3184.

Bianchi S, Stimpson CD, Bauernfeind AL, Schapiro SJ, Baze WB, McArthur MJ, Bronson E, Hopkins WD, Semendeferi K, Jacobs B, Hof PR, Sherwood CC. 2013. Dendritic Morphology of Pyramidal Neurons in the Chimpanzee Neocortex: Regional Specializations and Comparison to Humans. Cereb Cortex. 23:2429–2436.

Brodmann K. 1909. Vergleichende Lokalisationslehre der Großhirnrinde in ihren Prinzipien dargestellt auf Grund des Zellenbaues. Leipzig: Johannes Ambrosius Barth Verlag.

Buckner RL, Krienen FM. 2013. The evolution of distributed association networks in the human brain. Trends in Cognitive Sciences. 17:648–665.

Buzsáki G, Mizuseki K. 2014. The log-dynamic brain: how skewed distributions affect network operations. Nat Rev Neurosci. 15:264–278.

Cauli B, Audinat E, Lambolez B, Angulo MC, Ropert N, Tsuzuki K, Hestrin S, Rossier J. 1997. Molecular and Physiological Diversity of Cortical Nonpyramidal Cells. J Neurosci. 17:3894–3906.

Caviness VS, Bhide PG, Nowakowski RS. 2008. Histogenetic Processes Leading to the Laminated Neocortex: Migration Is Only a Part of the Story. Dev Neurosci. 30:82–95.

Charvet CJ, Cahalane DJ, Finlay BL. 2015. Systematic, Cross-Cortex Variation in Neuron Numbers in Rodents and Primates. Cereb Cortex. 25:147–160.

Charvet CJ, Finlay BL. 2014. Evo-devo and the primate isocortex: the central organizing role of intrinsic gradients of neurogenesis. Brain Behav Evol. 84:81–92.

Chaudhuri R, Knoblauch K, Gariel M-A, Kennedy H, Wang X-J. 2015. A Large-Scale Circuit Mechanism for Hierarchical Dynamical Processing in the Primate Cortex. Neuron. 88:419–431.

Chen ZJ, He Y, Rosa-Neto P, Germann J, Evans AC. 2008. Revealing Modular Architecture of Human Brain Structural Networks by Using Cortical Thickness from MRI. Cereb Cortex. 18:2374–2381.

Chen ZJ, He Y, Rosa-Neto P, Gong G, Evans AC. 2011. Age-related alterations in the modular organization of structural cortical network by using cortical thickness from MRI. NeuroImage. 56:235–245.

Chklovskii DB, Schikorski T, Stevens CF. 2002. Wiring Optimization in Cortical Circuits. Neuron. 34:341–347.

DeFelipe J. 2011. The evolution of the brain, the human nature of cortical circuits, and intellectual creativity. Front Neuroanat. 5:29.

Dégenètais E, Thierry A-M, Glowinski J, Gioanni Y. 2002. Electrophysiological Properties of Pyramidal Neurons in the Rat Prefrontal Cortex: An In Vivo Intracellular Recording Study. Cereb Cortex. 12:1–16.

Dehaene S, Changeux J-P, Naccache L. 2011. The Global Neuronal Workspace Model of Conscious Access: From Neuronal Architectures to Clinical Applications. In: Dehaene S,, Christen Y, editors. Characterizing Consciousness: From Cognition to the Clinic? Berlin, Heidelberg: Springer. p. 55–84.

Dehaene S, Kerszberg M, Changeux J-P. 1998. A neuronal model of a global workspace in effortful cognitive tasks. PNAS. 95:14529–14534.

Dombrowski SM, Hilgetag CC, Barbas H. 2001. Quantitative Architecture Distinguishes Prefrontal Cortical Systems in the Rhesus Monkey. Cereb Cortex. 11:975–988.

Douglas RJ, Martin KAC. 2007. Mapping the Matrix: The Ways of Neocortex. Neuron. 56:226–238.

Elston GN. 2000. Pyramidal Cells of the Frontal Lobe: All the More Spinous to Think With. J Neurosci. 20:RC95-RC95.

Elston GN. 2003. Cortex, Cognition and the Cell: New Insights into the Pyramidal Neuron and Prefrontal Function. Cereb Cortex. 13:1124–1138.

Elston GN. 2007. Specialization of the Neocortical Pyramidal Cell during Primate Evolution. In: Kaas JH, editor. Evolution of Nervous Systems. Oxford: Academic Press. p. 191–242.

Elston GN, Benavides-Piccione R, DeFelipe J. 2001. The Pyramidal Cell in Cognition: A Comparative Study in Human and Monkey. J Neurosci. 21:RC163-RC163.

Elston GN, Benavides-Piccione R, DeFelipe J. 2005. A Study of Pyramidal Cell Structure in the Cingulate Cortex of the Macaque Monkey with Comparative Notes on Inferotemporal and Primary Visual Cortex. Cereb Cortex. 15:64–73.

Elston GN, Benavides-Piccione R, Elston A, Manger P, Defelipe J. 2011a. Pyramidal cells in prefrontal cortex of primates: marked differences in neuronal structure among species. Front Neuroanat. 5:2.

Elston GN, Oga T, Okamoto T, Fujita I. 2011b. Spinogenesis and pruning in the anterior ventral inferotemporal cortex of the macaque monkey: an intracellular injection study of layer III pyramidal cells. Front Neuroanat. 5:42.

Elston GN, Okamoto T, Oga T, Dornan D, Fujita I. 2010. Spinogenesis and pruning in the primary auditory cortex of the macaque monkey (Macaca fascicularis): An intracellular injection study of layer III pyramidal cells. Brain Research. 1316:35–42.

Elston GN, Rockland KS. 2002. The Pyramidal Cell of the Sensorimotor Cortex of the Macaque Monkey: Phenotypic Variation. Cereb Cortex. 12:1071–1078.

Elston GN, Rosa MG. 1997. The occipitoparietal pathway of the macaque monkey: comparison of pyramidal cell morphology in layer III of functionally related cortical visual areas. Cereb Cortex. 7:432–452.

Elston GN, Rosa MG. 1998. Morphological variation of layer III pyramidal neurones in the occipitotemporal pathway of the macaque monkey visual cortex. Cereb Cortex. 8:278–294.

Elston GN, Tweedale R, Rosa MGP. 1999a. Supragranular pyramidal neurones in the medial posterior parietal cortex of the macaque monkey: morphological heterogeneity in subdivisions of area 7. NeuroReport. 10:1925–1929.

Elston GN, Tweedale R, Rosa MGP. 1999b. Cortical integration in the visual system of the macaque monkey: large-scale morphological differences in the pyramidal neurons in the occipital, parietal and temporal lobes. Proceedings of the Royal Society of London B: Biological Sciences. 266:1367–1374.

Ercsey-Ravasz M, Markov NT, Lamy C, Van Essen DC, Knoblauch K, Toroczkai Z, Kennedy H. 2013. A Predictive Network Model of Cerebral Cortical Connectivity Based on a Distance Rule. Neuron. 80:184–197.

Evans AC. 2013. Networks of anatomical covariance. NeuroImage, Mapping the Connectome. 80:489–504.

Felleman DJ, Van Essen DC. 1991. Distributed hierarchical processing in the primate cerebral cortex. Cerebral Cortex. 1:1–47.

Germuska M, Saha S, Fiala J, Barbas H. 2006. Synaptic Distinction of Laminar-specific Prefrontal-temporal Pathways in Primates. Cereb Cortex. 16:865–875.

Ghashghaei HT, Hilgetag CC, Barbas H. 2007. Sequence of information processing for emotions based on the anatomic dialogue between prefrontal cortex and amygdala. NeuroImage. 34:905–923.

Gong G, He Y, Chen ZJ, Evans AC. 2012. Convergence and divergence of thickness correlations with diffusion connections across the human cerebral cortex. NeuroImage. 59:1239–1248.

Goñi J, Heuvel MP van den, Avena-Koenigsberger A, Mendizabal NV de, Betzel RF, Griffa A, Hagmann P, Corominas-Murtra B, Thiran J-P, Sporns O. 2014. Resting-brain functional connectivity predicted by analytic measures of network communication. PNAS. 111:833–838.

Goulas A, Uylings HBM, Hilgetag CC. 2016. Principles of ipsilateral and contralateral cortico-cortical connectivity in the mouse. Brain Struct Funct. 1–15.

Goulas A, Uylings HBM, Stiers P. 2014. Mapping the Hierarchical Layout of the Structural Network of the Macaque Prefrontal Cortex. Cerebral Cortex. 24:1178–1194.

Harris KD, Shepherd GMG. 2015. The neocortical circuit: themes and variations. Nat Neurosci. 18:170–181.

He Y, Chen ZJ, Evans AC. 2007. Small-World Anatomical Networks in the Human Brain Revealed by Cortical Thickness from MRI. Cereb Cortex. 17:2407–2419.

Hilgetag CC, Grant S. 2010. Cytoarchitectural differences are a key determinant of laminar projection origins in the visual cortex. NeuroImage. 51:1006–1017.

Hilgetag CC, Medalla M, Beul SF, Barbas H. 2016. The primate connectome in context: Principles of connections of the cortical visual system. NeuroImage. 134:685–702.

Hof PR, Ungerleider LG, Adams MM, Webster MJ, Gattass R, Blumberg DM, Morrison JH. 1997. Callosally projecting neurons in the macaque monkey V1/V2 border are enriched in nonphosphorylated neurofilament protein. Visual Neuroscience. 14:981–987.

Hof PR, Ungerleider LG, Webster MJ, Gattass R, Adams MM, Sailstad CA, Morrison JH. 1996. Neurofilament protein is differentially distributed in subpopulations of corticocortical projection neurons in the macaque monkey visual pathways. J Comp Neurol. 376:112–127.

Lagae L, Gulyas B, Raiguel S, Orban GA. 1989. Laminar analysis of motion information processing in macaque V5. Brain Res. 496:361–367.

Larkum M. 2013. A cellular mechanism for cortical associations: an organizing principle for the cerebral cortex. Trends in Neurosciences. 36:141–151.

Lerch JP, Worsley K, Shaw WP, Greenstein DK, Lenroot RK, Giedd J, Evans AC. 2006. Mapping anatomical correlations across cerebral cortex (MACACC) using cortical thickness from MRI. NeuroImage. 31:993–1003.

Markov NT, Ercsey-Ravasz M, Lamy C, Gomes ARR, Magrou L, Misery P, Giroud P, Barone P, Dehay C, Toroczkai Z, Knoblauch K, Essen DCV, Kennedy H. 2013. The role of long-range connections on the specificity of the macaque interareal cortical network. PNAS. 110:5187–5192.

Markov NT, Ercsey-Ravasz M, Van Essen DC, Knoblauch K, Toroczkai Z, Kennedy H. 2013. Cortical High-Density Counterstream Architectures. Science. 342:1238406.

Markov NT, Ercsey-Ravasz MM, Ribeiro Gomes AR, Lamy C, Magrou L, Vezoli J, Misery P, Falchier A, Quilodran R, Gariel MA, Sallet J, Gamanut R, Huissoud C, Clavagnier S, Giroud P, Sappey-Marinier D, Barone P, Dehay C, Toroczkai Z, Knoblauch K, Van Essen DC, Kennedy H. 2014. A Weighted and Directed Interareal Connectivity Matrix for Macaque Cerebral Cortex. Cereb Cortex. 24:17–36.

Medalla M, Barbas H. 2006. Diversity of laminar connections linking periarcuate and lateral intraparietal areas depends on cortical structure. European Journal of Neuroscience. 23:161–179.

Medalla M, Lera P, Feinberg M, Barbas H. 2007. Specificity in Inhibitory Systems Associated with Prefrontal Pathways to Temporal Cortex in Primates. Cereb Cortex. 17:i136–i150.

Nieuwenhuys R, Broere CAJ. 2017. A map of the human neocortex showing the estimated overall myelin content of the individual architectonic areas based on the studies of Adolf Hopf. Brain Struct Funct. 222:465–480.

Nieuwenhuys R, Broere CAJ, Cerliani L. 2015. A new myeloarchitectonic map of the human neocortex based on data from the Vogt–Vogt school. Brain Struct Funct. 220:2551–2573.

Nowak LG, Munk MH, Girard P, Bullier J. 1995. Visual latencies in areas V1 and V2 of the macaque monkey. Vis Neurosci. 12:371–384.

Oswald MJ, Tantirigama ML, Sonntag I, Hughes SM, Empson RM. 2013. Diversity of layer 5 projection neurons in the mouse motor cortex. Front Cell Neurosci. 7:174.

Otsuka T, Kawaguchi Y. 2008. Firing-Pattern-Dependent Specificity of Cortical Excitatory Feed-Forward Subnetworks. J Neurosci. 28:11186–11195.

Pandya DN, Sanides F. 1973. Architectonic parcellation of the temporal operculum in rhesus monkey and its projection pattern. Zeitschrift für Anatomie und Entwicklungsgeschichte. 139:127–161.

Petroni F, Panzeri S, Hilgetag CC, Kötter R, Young MP. 2001. Simultaneity of responses in a hierarchical visual network. Neuroreport. 12:2753–2759.

Raiguel S, Van Hulle MM, Xiao D-K, Marcar VL, Orban GA. 1995. Shape and Spatial Distribution of Receptive Fields and Antagonistic Motion Surrounds in the Middle Temporal Area (V5) of the Macaque. European Journal of Neuroscience. 7:2064–2082.

Rempel-Clower NL, Barbas H. 2000. The laminar pattern of connections between prefrontal and anterior temporal cortices in the Rhesus monkey is related to cortical structure and function. Cerebral Cortex. 10:851–865.

Salvador R, Suckling J, Coleman MR, Pickard JD, Menon D, Bullmore E. 2005. Neurophysiological Architecture of Functional Magnetic Resonance Images of Human Brain. Cereb Cortex. 15:1332–1342.

Scholtens LH, Schmidt R, de Reus MA, van den Heuvel MP. 2014. Linking Macroscale Graph Analytical Organization to Microscale Neuroarchitectonics in the Macaque Connectome. J Neurosci. 34:12192–12205.

Seltzer B, Pandya DN. 1978. Afferent cortical connections and architectonics of the superior temporal sulcus and surrounding cortex in the rhesus monkey. Brain Research. 149:1–24.

Spruston N. 2008. Pyramidal neurons: dendritic structure and synaptic integration. Nat Rev Neurosci. 9:206–221.

Tewarie P, Hillebrand A, van Dellen E, Schoonheim MM, Barkhof F, Polman CH, Beaulieu C, Gong G, van Dijk BW, Stam CJ. 2014. Structural degree predicts functional network connectivity: A multimodal resting-state fMRI and MEG study. NeuroImage. 97:296–307.

Tewarie P, Steenwijk MD, Tijms BM, Daams M, Balk LJ, Stam CJ, Uitdehaag BMJ, Polman CH, Geurts JJG, Barkhof F, Pouwels PJW, Vrenken H, Hillebrand A. 2014. Disruption of structural and functional networks in long-standing multiple sclerosis. Hum Brain Mapp.

Van Essen DC, Drury HA, Dickson J, Harwell J, Hanlon D, Anderson CH. 2001. An Integrated Software Suite for Surface-based Analyses of Cerebral Cortex. J Am Med Inform Assoc. 8:443–459.

Vértes PE, Alexander-Bloch AF, Gogtay N, Giedd JN, Rapoport JL, Bullmore ET. 2012. Simple models of human brain functional networks. PNAS. 109:5868–5873.

von Economo C. 1927. Zellaufbau der Grosshirnrinde des Menschen. Berlin: Springer.

von Economo C. 2009. Cellular Structure of the Human Cerebral Cortex. Basel, Switzerland: Karger Medical and Scientific Publishers.

Young MP. 1992. Objective analysis of the topological organization of the primate cortical visual system. Nature. 358:152–155.

Yukie M. 1997. Organization of visual afferent connections to inferior temporal cortex, area TE, in the macaque monkey. In: Sakata H,, Mikami A,, Fuster J, editors. The association cortex, structure and function. Amsterdam, Netherlands: Harwood Academic. p. 247–258.

Yuste R. 2010. Dendritic Spines. MIT Press.

Zikopoulos B, Barbas H. 2010. Changes in Prefrontal Axons May Disrupt the Network in Autism. The Journal of Neuroscience. 30:14595–14609.

Zikopoulos B, Barbas H. 2013. Altered neural connectivity in excitatory and inhibitory cortical circuits in autism. Front Hum Neurosci. 7:609.

Zilles K, Amunts K. 2009. Receptor mapping: architecture of the human cerebral cortex. Curr Opin Neurol. 22:331–339.

Tables

Table 1. Correspondence of cortical areas across parcellations.

Connectivity data were published in the M132 parcellation (Markov et al., 2014), while the morphological measures were extracted from reports using alternative parcellations of the macaque cortex. This table shows how areas were matched across parcellations and indicates precise references for morphological measures in each area. ER97, Elston and Rosa 1997; ER98, Elston and Rosa 1998; E99a, Elston et al., 1999a; E99b, Elston et al., 1999b; E00, Elston 2000; E01, Elston et al. 2001; ER02, Elston and Rockland 2002; E05, Elston et al. 2005; E10, Elston et al. 2010; E11a, Elston et al. 2011a; E11b, Elston et al. 2011b.

Area label in M132	Area label in morphological measures reference	Reference
3	3b	ER02
5	5	ER02
9	9d	E11a
10	10	E00, E11a
11	11	E00
12	12	E11a
14	13	E11a
23	Posterior cingulate	E05
24a	Anterior cingulate	E05
24b	Anterior cingulate	E05
24c	Anterior cingulate	E05
24d	Anterior cingulate	E05
46v	46	E11a
7a	7a	ER97
7b	7b	ER02
7m	7m	E99a
core	A1	E10
F1	4	ER02
F2	6	ER02
LIP	LIPv	ER97
MT	MT	ER97
STPi	STP	E99b
TEad	TEa of Seltzer and Pandya, 1978; TEad(s) of Yukie, 1997; PIT of Felleman and Van Essen, 1991	E99b, E05
TEav	TE	E11b
TEO	TEO	ER98
TEpd	TEpd	E11b
V1	V1	ER97, ER98, E05
V2	V2	ER97, ER98, E01
V4	V4	ER98

Table 2. Correlation between structural measures.

Pearson correlation coefficients and associated p-values for correlations between neuron density and the morphological measures. Bonferroni correction for multiple tests results in an adjusted significance threshold of $\alpha_{adj} = 0.05/10 = 0.005$.

	Neuron density		**Soma size**		**Spine count**		**Spine density**	
	r	p-value	r	p-value	r	p-value	r	p-value
Soma size	-0.83	<0.0001	-	-				
Spine count	-0.64	0.0007	0.84	0.0002	-	-		
Spine density	-0.62	0.0012	0.74	0.0025	0.79	0.0007	-	-
Dendritic tree size	-0.62	0.0009	0.61	0.0197	0.71	0.0044	0.28	0.3327

Table 3. Structural measures in connected and unconnected pairs of areas.

Absolute values of relative structural measures are averaged across area pairs without (absent) and with (present) a linking projection. T-statistics, p-values and effect size r are results of two-tailed independent samples t-tests comparing the two respective distributions for equal means. Values for the area-based measures have been reported previously (Beul et al., 2017). See Figure 3 for box plots of the underlying distributions.

	Mean absent projections	**Mean present projections**	**t-statistic**	**p-value**	**r**
Area-based measures					
$\lvert\text{log-ratio}_{density}\rvert$	0.49	0.24	$t_{(1126)} = 13.8$	<.001	0.38
$\lvert\text{log-ratio}_{thickness}\rvert$	0.20	0.14	$t_{(2608)} = 11.5$	<.001	0.22
Euclidean distance [mm]	32.9	25.7	$t_{(2608)} = 15.1$	<.001	0.28
Cellular morphological measures					
$\lvert\Delta_{soma\ size}\rvert$ [µm²]	69.8	41.6	$t_{(334)} = 5.8$	<.001	0.30
$\lvert\Delta_{spine\ count}\rvert$ [#]	3 670.4	2 727.4	$t_{(376)} = 4.2$	<.001	0.21
$\lvert\Delta_{spine\ density}\rvert$ [#/10µm]	9.5	7.3	$t_{(376)} = 4.0$	<.001	0.20
$\lvert\Delta_{tree\ size}\rvert$ [µm²]	50 934.2	39 635.1	$t_{(418)} = 3.4$	<.001	0.16

Table 4. Classification of connection existence by logistic regression.

We performed five binary logistic regression analyses (enumerated in brackets), each including a different set of the structural measures as covariates and connectivity (grouped into 'absent' and 'present' connections) as the dependent variable. Bold-faced covariates significantly contributed to classification performance as indicated by the p-value. Across all regression analyses, absolute neuron density ratio and Euclidean distance consistently emerged as meaningful predictors. Absolute soma size difference, which contributed significantly within the subset of morphological measures (2), was no relevant predictor if absolute neuron density ratio was included as well (4), but did remain so in combination with Euclidean distance (5).

	Regression covariates	Regression coefficient	Wald statistic	p-value
	Area-based measures			
(1)	**$\lvert$log-ratio$_{density}\rvert$**	-0.584	30.72	<.001
	$\lvert$log-ratio$_{thickness}\rvert$	0.115	1.35	0.245
	Euclidean distance	-0.724	94.02	<.001
	Cellular morphological measures			
(2)	**$\lvert\Delta_{soma\ size}\rvert$**	-0.387	7.18	0.007
	$\lvert\Delta_{spine\ count}\rvert$	-0.363	2.55	0.110
	$\lvert\Delta_{spine\ density}\rvert$	-0.139	0.45	0.505
	$\lvert\Delta_{tree\ size}\rvert$	-0.202	2.08	0.149
	Combinations of all measures			
(3)	**$\lvert$log-ratio$_{density}\rvert$**	-0.763	12.26	<.001
	$\lvert$log-ratio$_{thickness}\rvert$	0.242	1.33	0.249
	Euclidean distance	-0.794	24.66	<.001
	$\lvert\Delta_{soma\ size}\rvert$	0.020	0.01	0.927
	$\lvert\Delta_{spine\ count}\rvert$	-0.436	2.41	0.120
	$\lvert\Delta_{spine\ density}\rvert$	0.179	0.48	0.487
	$\lvert\Delta_{tree\ size}\rvert$	0.047	0.06	0.806
(4)	**$\lvert$log-ratio$_{density}\rvert$**	-0.745	19.68	<.001
	$\lvert\Delta_{soma\ size}\rvert$	-0.49	0.08	0.772
(5)	**Euclidean distance**	-0.839	44.25	<.001
	$\lvert\Delta_{soma\ size}\rvert$	-0.485	13.57	<.001

Table 5. Correlation between projection strength and structural measures.

Pearson correlation coefficients and associated p-values for correlations between projection strength, ln(FLNe), and absolute values of relative structural measures. Correlations were assessed both for each measure independently (individual correlation) and while accounting for all other six measures (partial correlation). See Figure 5 for scatter plots of the underlying distributions.

	Individual correlation		**Partial correlation**	
	r	p-value	r	p-value
$\lvert$log-ratio$_{density}\rvert$	-0.23	<0.0001	-0.20	0.0196
$\lvert$log-ratio$_{thickness}\rvert$	-0.12	<0.0001	0.06	0.5085
Euclidean distance	-0.39	<0.0001	-0.41	<0.0001
$\lvert\Delta_{soma\ size}\rvert$	-0.19	0.0090	<|0.01|	0.9553
$\lvert\Delta_{spine\ count}\rvert$	-0.26	0.0002	-0.02	0.8533
$\lvert\Delta_{spine\ density}\rvert$	-0.25	0.0004	-0.17	0.0408
$\lvert\Delta_{tree\ size}\rvert$	-0.11	0.1026	-0.04	0.6376

Table 6. Correlation between laminar projection patterns and structural measures.

Pearson correlation coefficients and associated p-values for correlations between N_{SG}% and relative structural measures. Correlations were assessed both for each measure independently (individual correlation with N_{SG}%) and while accounting for five other measures (partial correlation with N_{SG}%). Euclidean distance could not be correlated with N_{SG}%, because it is an undirected measure. Instead, the individual correlation of Euclidean distance with laminar patterns (marked '*') was computed using $\lvert N_{SG}\%\rvert$, which indicates deviation from bilaminar projection patterns. Accordingly, we also computed a partial correlation accounting for all seven structural measures at once, which had to include the absolute values of the relative structural measures (partial correlation with $\lvert N_{SG}\%\rvert$). See Figure 6 for scatter plots of the underlying distributions.

	Individual correlation with NSG%		**Partial correlation with NSG%**			**Partial correlation with |NSG%|**	
	r	p-value	r	p-value		r	p-value
log-ratio$_{density}$	0,44	<0,0001	0,44	<0,0001	$\lvert$log-ratio$_{density}\rvert$	0,34	0,0008
log-ratio$_{thickness}$	-0,30	<0,0001	-0,02	0,8774	$\lvert$log-ratio$_{thickness}\rvert$	-0,09	0,4026
Euclidean distance*	0,06	0,0588	-/-	-/-	Euclidean distance	-0,08	0,4174
$\Delta_{soma\ size}$	-0,45	<0,0001	-0,09	0,3720	$\lvert\Delta_{soma\ size}\rvert$	0,24	0,0179
$\Delta_{spine\ count}$	-0,56	<0,0001	-0,38	0,0001	$\lvert\Delta_{spine\ count}\rvert$	0,25	0,0144
$\Delta_{spine\ density}$	-0,32	0,0001	0,37	0,0002	$\lvert\Delta_{spine\ density}\rvert$	-0,05	0,6310
$\Delta_{tree\ size}$	-0,57	<0,0001	-0,01	0,8883	$\lvert\Delta_{tree\ size}\rvert$	0,17	0,0868

Table 7. Correlation between area degree and structural measures.

Pearson correlation coefficients and associated p-values for correlations between area degree (number of maintained connections) and structural measures for each area. Correlations were assessed both for each measure independently (individual correlation) and while accounting for the other five measures (partial correlation). Euclidean distance could not be included because it is a relational property not defined for individual areas. Bonferroni correction for multiple tests results in an adjusted significance threshold of $\alpha_{adj} = 0.05/6 = 0.0083$ for the individual correlations. Individual correlations of neuron density and cortical thickness with degree have been reported previously (Beul et al., 2017). See Figure 7 for scatter plots of the underlying distributions.

	Individual correlation		**Partial correlation**	
	r	p-value	r	p-value
Neuron density	-0.60	0.002	-0.65	0.084
Cortical thickness	0.38	0.041	0.54	0.167
Soma size	0.33	0.243	-0.60	0.116
Spine count	0.32	0.269	0.37	0.363
Spine density	0.21	0.477	-0.52	0.188
Dendritic tree size	0.50	0.057	0.14	0.748